Unraveling the Anomalous Grain Size Dependence of Cavitation

J. W. Wilkerson and K. T. Ramesh

Unraveling the anomalous grain size dependence of cavitation

J.W. Wilkerson[1] and K.T. Ramesh[2]

[1] *Department of Mechanical Engineering, University of Texas at San Antonio, TX, USA*
[2] *Hopkins Extreme Materials Institute, The Johns Hopkins University, Baltimore, MD, USA*
(Dated: October 28, 2016)

Experimental studies have identified an anomalous grain size dependence associated with the critical tensile pressure that a metal may sustain before catastrophic failure by cavitation processes. Here we derive the first quantitative theory (and its associated closed-form solution) capable of explaining this phenomena. The theory agrees well with experimental measurements and atomistic calculations over a very wide range of conditions. Utilizing this theory, we are able to map out three distinct regimes in which the critical tensile pressure for cavitation failure i) increases with decreasing grain size in accordance with conventional wisdom, ii) non-intuitively decreases with decreasing grain size, and iii) is independent of grain size. The theory also predicts microscopic signatures of the cavitation process which agree with available data.

Cavitation instabilities may be induced in most forms of matter, e.g. fluids [1, 2], polymers [3, 4], amorphous solids [5–7], deuterated solvents [8], liquid helium [9], biological tissue [10], engineering materials [11], through the rapid deposition of high-intensity energy, e.g. by impact [11], laser irradiation [12], ultrasound [2], hydrodynamic machinery [3], the snapping claw of the *Alpheus heterochaelis* [13]. While many of these stimuli are somewhat specialized, impact processes are ubiquitous throughout nature: from the woodpecker *(Picoides)*, whose skull and beak have evolved over millennia to sustain $1000\ g$ decelerations without inducing brain injury [14], to the planetary and asteroidal impacts that have shaped our Solar System [15], as well as in many modern technologies.

For a sufficiently energetic impact, shock compression waves are generated at the impact source and propagate throughout the impacting bodies. These shock waves interact with surfaces and interfaces to produce complex mechanical wave phenomena, which can cause regions of the bodies to experience very high tensile pressures. When subjected to this tensile pressure, many materials tend to fracture by cavitation processes. This overall process is commonly termed spall failure in the shock physics community, and the maximum tensile pressure the material may sustain before subsequent catastrophic fracture is termed the spall strength [11]. While seemingly specialized, such experiments are of fundamental interests as they probe cavitation processes on the ultra-short timescales directly relevant to atomistic calculations.

Recently, a number of experimental studies [16–20] have identified an anomalous grain size dependence, i.e. a *smaller is weaker* behavior, in spall strength. Such observations are perplexing as they run counter to the typical *smaller is stronger* size-effects observed in a range of materials and phenomena [21–23]. While smaller is weaker anomalies have been observed [24–27] in materials with extremely small grain sizes, e.g. a few nanometers; cavitation failure is unusual in that it exhibits this anomalous behavior over a much larger range of grain sizes, e.g. nanometers to millimeters.

For grain sizes, d_G, larger than several nanometers size-effects in strength generally scale according to the well-known Hall-Petch law:

$$\sigma_y = \sigma_0 + \frac{k_y}{\sqrt{d_G}}, \tag{1}$$

where σ_y denotes the yield strength, a material property characterizing the resistance to permanent plastic deformation, and σ_0 and k_y are model parameters (e.g. $\sigma_0 = 200$ MPa and $k_y = 0.14$ MPa$\sqrt{\text{m}}$ for copper). Intuitively, Eq. (1) may lead one to presume that spall strength, Σ_m^*, likely scales with grain size similarly to yield strength, i.e. *smaller is stronger*; however, experimental measurements [16–20] show the opposite trend. One extreme example of this non-intuitive grain size dependence, i.e. $\partial \Sigma_m^*/\partial d_G > 0$, is the experimental observation that the spall strength of single crystal, i.e. $d_G \to \infty$, copper is a factor of $2-3$ higher [28] than the spall strength of coarse-grained polycrystalline copper with $d_G \sim 100\ \mu$m (c.f. symbols in Fig. 1). Contradictingly, atomistic calculations [29, 30] of spall strength of nanocrystalline materials predict the more intuitively expected *smaller is stronger* behavior, i.e. $\partial \Sigma_m^*/\partial d_G < 0$. Here we derive the first quantitative theory capable of explaining these contradicting observations.

Consider an isolated, infinitesimally small spherical cavity of radius $A \to 0$ in an otherwise infinite elastic-plastic medium whose resistance to elastic and plastic deformation are characterized by the modulus of elasticity, E, and the yield strength, i.e. σ_y in Eq. (1), respectively. Extending a previous analysis [31] to account for grain size here, the critical tensile pressure $\mathcal{R}_y$ required to initiate growth of this infinitesimally small cavity is

$$\mathcal{R}_y = \frac{2}{3}\left(\sigma_0 + \frac{k_y}{\sqrt{d_G}}\right)\left\{1 - \ln\frac{3}{2}\left(\frac{\sigma_0}{E} + \frac{k_y}{E\sqrt{d_G}}\right)\right\}, \tag{2}$$

where $\mathcal{R}_y$ can be interpreted as the critical tensile pressure required to initiate cavitation. The critical pressure for cavitation scales similarly to the Hall-Petch law, i.e. $\partial \mathcal{R}_y/\partial d_G < 0$; however, the scaling is a bit weaker, i.e.

$|\partial\mathcal{R}_y/\partial d_G| \lesssim |\partial\sigma_y/\partial d_G|$, due to the negative logarithmic term in Eq. (2).

The derivation associated with Eq. (2) assumes a pre-existing, albeit infinitesimally small, defect from which cavitation is nucleated. Consider now a more homogeneous nucleation of free-volume that occurs when a perfect lattice is severely expanded to the point that the intermolecular forces holding the lattice together begin to decrease with increasing lattice parameter. At this critical tensile pressure, $\mathcal{R}_{eos}$, the lattice becomes unstable. Here we assume that the spall strength of any material can not exceed this *ideal spall strength*, i.e. $\Sigma_m^* \leq \mathcal{R}_{eos}$.

For typical metals, $\mathcal{R}_{eos}$ is one or two orders of magnitude greater than $\mathcal{R}_y$, e.g. the room-temperature value of $\mathcal{R}_{eos}$ was approximated to be 22.5 GPa for copper [32]. However, cavitation nucleation is likely to be a stochastic process that at best may be bounded by these two approximations. Following this argument, we assume that the critical nucleation pressure $\mathcal{R}_{cr}^\alpha$ for any randomly selected potential cavitation nucleation site associated with the α-family of sites follows a bounded power-law probability distribution function:

$$g_\alpha(\mathcal{R}_{cr}^\alpha) = (\beta^\alpha - 1)\frac{\langle\mathcal{R}_{cr}^\alpha - \mathcal{R}_y\rangle^{\beta_\alpha - 1}}{(\mathcal{R}_{eos} - \mathcal{R}_y)^{\beta_\alpha}}, \qquad (3)$$

for $\mathcal{R}_{cr}^\alpha \leq \mathcal{R}_{eos}$ with $\langle\cdot\rangle$ denoting Macaulay brackets. The associated cumulative distribution function is $G_\alpha(\mathcal{R}_{cr}^\alpha) = \langle\mathcal{R}_{cr}^\alpha - \mathcal{R}_y\rangle^{\beta_\alpha}/(\mathcal{R}_{eos} - \mathcal{R}_y)^{\beta_\alpha}$ with β_α denoting the power-law exponent associated with the α-family of sites. We choose $\beta_\alpha = 3$ and $\beta_\alpha = 10$, respectively, for families of nucleation sites along grain boundaries and within grain interiors. The rationale for this choice is the observation that grain boundaries are preferred nucleation sites over grain interiors at lower tensile pressures [33].

Once the cavitation process is initiated, unstable growth of the cavity proceeds restrained only by the inertial mass density ($\rho = 8960$ kg m^{-3} for copper) of the solid material surrounding the cavity. Conservation of radial momentum gives rise to the non-linear differential equation governing the dynamic growth of an isolated spherical cavity of radius a, i.e.

$$\rho a\ddot{a} + \frac{3}{2}\rho\dot{a}^2 = \langle\Sigma_m - \mathcal{R}_{cr}^\alpha\rangle, \qquad (4)$$

with $\Sigma_m \triangleq -p$. For a constant tensile pressure rate, e.g. $\Sigma_m = \dot{\Sigma}_m t$ with t denoting time, there exists an analytic solution [31] of Eq. (4):

$$a = \sqrt{\frac{8}{33}\frac{\langle\Sigma_m - \mathcal{R}_{cr}^\alpha\rangle^{\frac{3}{2}}}{\dot{\Sigma}_m\sqrt{\rho}}}. \qquad (5)$$

Following nucleation, the characteristic time t_f required for cavities to grow to a sufficient critical size a_f such that they begin to coalesce and trigger catastrophic fracture is $t_f \sim \sqrt[3]{\rho a_f^2/\dot{\Sigma}_m}$ according to Eq. (5). For metals subject
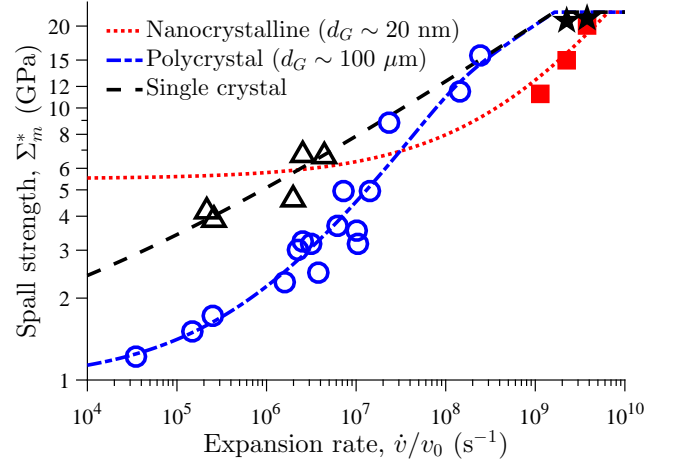

FIG. 1: Agreement of theory (lines), i.e. Eq. (10), with experimental measurements (open symbols) as well as atomistic calculations (closed symbols) for high purity copper. The single crystal $-\triangle-$ and coarse-grained polycrystal $-\circ-$ experimental data are reported in [28] and [12, 34], respectively. The single crystal $-\star-$ and nanocrystalline $-\blacksquare-$ atomistic calculations are reported in [32] and [30], respectively.

to typical conditions: $\rho \sim \mathcal{O}(10^4$ kg m$^{-3})$, $a_f \sim \mathcal{O}(1$ μm), and $\dot{\Sigma}_m \sim \mathcal{O}(10^{-2}-1$ GPa/ns) implying $t_f \sim \mathcal{O}(1-10$ ns). For everyday life, this timescale is very short and may be effectively treated as instantaneous. However, for energetic impacts this timescale may be comparable to timescales associated with expansion rates.

Consider now the simplest possible equation of state:

$$\Sigma_m = K_0\frac{\Delta v_e}{v_0}, \qquad (6)$$

where $K_0 = 140$ GPa denotes the bulk modulus (of copper) at reference conditions, v_0 denotes specific volume at reference conditions, and Δv_e denotes the portion of the change in specific volume, i.e. $\Delta v \triangleq v - v_0$, that is elastically recoverable. Since cavitation involves the generation of irrecoverable free-volume, a portion of the change in specific volume is irrecoverable, i.e. Δv_p, with $\Delta v = \Delta v_e + \Delta v_p$. Given a distribution of $\hat\alpha$ distinct families of spherical cavities whose populations are governed by Eq. (3), the irrecoverable portion of the change in specific volume may be expressed as

$$\frac{\Delta v_p}{v_o} = \frac{4}{3}\pi\sum_{\alpha=1}^{\hat\alpha} N_\alpha\int_0^\infty a^3 g_\alpha(\mathcal{R}_{cr}^\alpha)d\mathcal{R}_{cr}^\alpha, \qquad (7)$$

with N_α denoting the potential number of α-family cavitation nucleation sites per unit initial volume. For simplicity, we limit ourselves here to $\hat\alpha = 2$ with $\alpha = 1$ and $\alpha = 2$ representing nucleation sites at grain boundaries and grain interiors, respectively. For grain interiors, we chose $N_2 = 5000$ μm^{-3}; however, the nucleation site density associated with grain boundaries is expected to
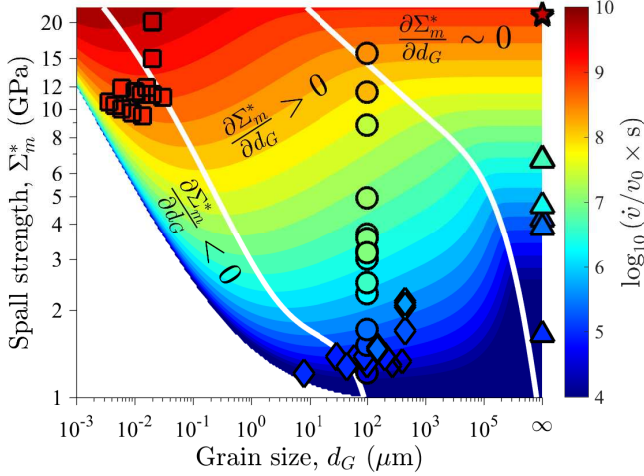
FIG. 2: Contour map demonstrating the anomalous grain size dependence of spall strength as a function of expansion rate as predicted by our theory, i.e. Eq. (10). The theoretically predicted trends agree with grain size dependence experimental studies $-\diamond-$ and molecular dynamics studies $-\square-$ reported in [16–20] and [29, 30], respectively. The thick white lines partition the space into regions in which spall strength i) follows Hall-Petch behavior, i.e. $\partial \Sigma_m^*/\partial d_G < 0$, ii) scales inversely to Hall-Petch phenomena, i.e. $\partial \Sigma_m^*/\partial d_G > 0$, and iii) insensitivity with respect to grain size, i.e. $\partial \Sigma_m^*/\partial d_G \sim 0$. Experimental data presented in Fig. (1) is shown as well.

roughly scale with the grain boundary surface area $\mathcal{O}(d_G^2)$ to grain volume $\mathcal{O}(d_G^3)$ ratio, i.e.

$$N_1 = N_{GB}^0 \times \frac{d_G^0}{d_G}, \tag{8}$$

where $N_{GB}^0 = 10 \ \mu\text{m}^{-3}$ denotes the grain boundary site density for coarse-grained, i.e. $d_G^0 = 100 \ \mu\text{m}$, copper.

Equations (4) and (6)–(8) now constitute a full set of differential equations necessary to compute the isothermal equation of state ($p - v - \dot{v} - T$) for a prescribed expansion, i.e. $v = f(t)$, with the maximum tensile pressure achieved being the spall strength, Σ_m^*. Our theory predicts that the spall strength of nanocrystalline metals ($d_g \sim 20$ nm) is higher than single crystals (in accordance with Hall-Petch behavior) at low expansion rates; however, at higher expansion rates ($\gtrsim 10^6 - 10^7$ s^{-1}) the behavior non-intuitively reverses due to the very low rate-sensitivity, i.e. $m^* \triangleq \partial \ln \Sigma_m^*/\partial \ln(\dot{v}/v_0)$, of nanocrystalline metals (see Fig. 1). A similar trend has been experimentally measured for iron [35]. This low rate-sensitivity m^* is a direct consequence of the very high number of grain boundary nucleation sites present in nanocrystalline metals, which enable rapid stress relaxation. The theory also predicts a similar transition in the spall strengths of coarse-grained polycrystals as compared to nanocrystalline (see Fig. 1). While this trend has yet to be experimentally confirmed, it is some-

what supported by the extrapolation of the data on iron [35]. Lastly, the theory predicts the convergence of spall strength of single crystals and coarse-grained polycrstals at sufficiently high expansion rates ($\gtrsim 10^8$ s^{-1}), and perhaps an achievement of the *ideal spall strength* at ultra high expansion rates ($\gtrsim 10^9$ s^{-1}) where microstructure becomes irrelevant. Interestingly, grain size independence has also been observed in growth dynamics of Rayleigh-Taylor instabilities at ultra high pressures [36].

Figure 2 identifies three distinct regions: i) correspondence with Hall-Petch behavior, i.e. $\partial \Sigma_m^*/\partial d_G < 0$, for ultra-fine-grain sizes ($d_G \sim 0.1 - 1 \ \mu\text{m}$) at high expansion rates ($\dot{v}/v_0 \sim 10^4 - 10^6$ s^{-1}) as well as nanocrystalline materials ($d_G \lesssim 100$ nm) at extreme expansion rates ($\dot{v}/v_0 \sim 10^6 - 10^8$ s^{-1}), ii) the non-intuitive, inverse Hall-Petch behavior, i.e. $\partial \Sigma_m^*/\partial d_G > 0$, for coarse-grained ($d_G \sim 100 \ \mu\text{m}$) and fine-grained ($d_G \sim 10 \ \mu\text{m}$) structures at high expansion rates as well as for ultra-fine-grain sizes at extreme rates, and iii) insensitivity, i.e. $\partial \Sigma_m^*/\partial d_G \sim 0$, for coarse-grained and fine-grained structures at ultra high expansion rates.

The remarkable agreement of this theory with both experimental and atomistic calculations as demonstrated by Figs. 1 and 2 validates our key assumptions and choice of parameters. The microscopic information regarding the total and relative number of cavities nucleated at grain boundaries versus within grain interiors provides a second layer of validation as well as deeper insights. The number of α-family cavities nucleated per unit volume during cavitation may be determined from the associated cumulative distribution function, i.e. $N_{nuc}^\alpha = N_\alpha G_\alpha(\Sigma_m^*)$, and the total number density is denoted as $N_{nuc} \triangleq \sum_{\alpha=1}^{\hat{\alpha}} N_{nuc}^\alpha$. Figure 3 shows theory predictions of the total number density N_{nuc} of nucleated cavities as a function of grain size and the spall strength achieved. Despite the simplistic nature of our theory, the predicted number densities compare well to those of experimental measurements. For example, [12, 16, 33] analyzed the number density of cavities near spall fracture surfaces and observed $N_{nuc} \sim \mathcal{O}(10^{-2} - 10^{-1} \ \mu\text{m}^{-3})$ for polycrystals ($d_G \sim 100 \mu\text{m}$) that exhibited moderate spall strength, i.e. $\Sigma_m^* \sim 1.5 - 2.5$ GPa, and $N_{nuc} \sim \mathcal{O}(1 \ \mu\text{m}^{-3})$ for polycrystals exhibiting high spall strengths, i.e. $\Sigma_m^* \sim 5 - 9$ GPa. Under similar conditions, our theory predicts values of $N_{nuc} \sim \mathcal{O}(10^{-2} \ \mu\text{m}^{-3})$ and $N_{nuc} \sim \mathcal{O}(1 \ \mu\text{m}^{-3})$, respectively, c.f. Fig. 3. A significantly higher cavity number density of $N_{nuc} \sim \mathcal{O}(10^5 \ \mu\text{m}^{-3})$ has been reported in atomistic calculations [30] for nanocrystalline ($d_G \sim 20$ nm) copper exhibiting an extremely high spall strength, i.e. $\Sigma_m^* \gtrsim 12$ GPa, with our theory predicting $N_{nuc} \sim \mathcal{O}(10^4 \ \mu\text{m}^{-3})$ under these conditions, c.f. Fig. 3. Lastly, the theory predicts the experimentally observed [33] transition from predominantly transgranular fracture to predominantly intergranular fracture with decreasing grain size as indicated by partitioned regions of Fig. 3.

Deeper insights into the underlying physics govern-

ing this complex behavior may be elucidated through a closed-form approximate solution of Eqs. (4), (6), and (7) by employing Eq. (5) as a sufficiently accurate approximation for a constant expansion rate, i.e.

$$\frac{\Delta v_p}{v_0} = \frac{\hat{\kappa} v_0^3 c_B^3}{\dot{v}^3 K_0^{\frac{9}{2}}} \sum_{\alpha=1}^{\hat{\alpha}} \zeta_\alpha N_\alpha \frac{\langle \Sigma_m - \mathcal{R}_y \rangle^{\beta_\alpha + \frac{9}{2}}}{(\mathcal{R}_{eos} - \mathcal{R}_y)^{\beta_\alpha}}, \quad (9)$$

with $\zeta_\alpha = 2^{\beta_\alpha} (\beta_\alpha - 1) \Gamma(\beta_\alpha) \prod_{i=1}^{\beta_\alpha} (9 + 2i)^{-1}$ for $\beta_\alpha \neq 1$, $\zeta_\alpha = 1$ for $\beta_\alpha = 1$, $\hat{\kappa} \triangleq \frac{4}{3}\pi \left(\frac{8}{33}\right)^{\frac{3}{2}}$, and $c_B \triangleq \sqrt{K_0/\rho}$ denoting the bulk wave speed. The maximum tensile pressure, i.e. $\Sigma_m = \Sigma_m^*$, is achieved at the tensile inflection point, i.e. $\dot{\Sigma}_m = 0$. From time differentiation of Eq. (6) this condition is met for $\Delta \dot{v}_e = 0$, or equivalently $\dot{v} = \Delta \dot{v}_p$. Employing this condition along with time differentiation of Eq. (9) it follows that

$$\frac{\dot{v}}{v_0} = \sqrt[3]{\frac{\hat{\kappa} c_B^3}{K_0^{\frac{7}{2}}} \sum_{\alpha=1}^{\hat{\alpha}} \hat{\zeta}_\alpha N_\alpha \frac{\langle \hat{c}_\alpha^*(\Sigma_m^* - \mathcal{R}_y) \rangle^{\beta_\alpha + \frac{7}{2}}}{(\mathcal{R}_{eos} - \mathcal{R}_y)^{\beta_\alpha}}}, \quad (10)$$

with $\hat{\zeta}_\alpha \triangleq (\beta_\alpha + 9/2) \zeta_\alpha$ and $\hat{c}_\alpha^* \triangleq \frac{9 + 2\beta_\alpha}{7 + 2\beta_\alpha}$ being a factor that accounts for the softening generated by the finite, non-negligible value of $-K_0 \Delta v_p/v_0$ in Eq. (6) at $\Sigma_m = \Sigma_m^*$. Neglecting the significant and non-intuitive effects of grain size, a less general (effectively limited to single crystals) and less accurate ($\hat{c}_\alpha^*$ neglected) version of Eq. (10) was previously derived [37]. Excellent agreement between Eq. (10) and numerical solutions of our theory are shown in [38].

If there happens to be a single dominant family of cavities, i.e. $\frac{\Delta v_p}{v_o} \approx \frac{4}{3}\pi N_\alpha \int_0^\infty a^3 g_\alpha(\mathcal{R}_{cr}^\alpha) d\mathcal{R}_{cr}^\alpha$, then Eq. (10) may be inverted, i.e.

$$\Sigma_m^* = \mathcal{R}_y + \frac{K_0}{\hat{c}_\alpha^*} \sqrt[\hat{\beta}_\alpha]{\frac{(\mathcal{R}_{eos} - \mathcal{R}_y)^{\beta_\alpha}}{\hat{\kappa} c_B^3 K_0^{\beta_\alpha} \hat{\zeta}_\alpha N_\alpha} \left(\frac{\dot{v}}{v_0}\right)^{\frac{3}{\beta_\alpha}}}, \quad (11)$$

with $\hat{\beta}_\alpha \triangleq \beta_\alpha + \frac{7}{2}$. Expressed in this form, the anomalous grain size dependence may be understood better. The first term on the right hand side of Eq. (11), i.e. R_y, scales roughly as $d_G^{-1/2}$ in accordance with Hall-Petch phenomena. The second term scales with $N_\alpha^{-1/\hat{\beta}_\alpha}$, which according to Eq. (8) implies that this term scales as $d_G^{\hat{\beta}_\alpha}$ when grain boundary nucleation sites dominate. In particular, for our choice of $\beta_\alpha = 3$ this second term scales as $d_G^{6.5}$. This competition is at the heart of the anomalous grain size dependence associated with spall strength. A similar competition between a size-dependent nucleation criterion and time-dependent dynamics of cavity (defect) volume growth may govern anomalous cavitation phenomena in other forms of matter, e.g. [1, 2, 4, 6, 26], as well as other relaxation processes [26, 36, 39].

In summary, we have derived the first physics-based theory of cavitation in to explain the anomalous grain size dependence of spall strength with minimal unknown parameters, i.e. N_α and β_α. In particular, we identify
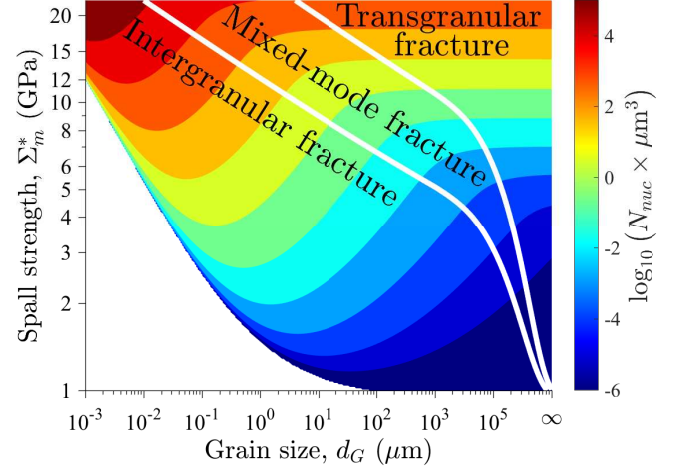

FIG. 3: Contour map demonstrating the predicted total number of cavities nucleated per unit volume, N_{nuc}, as a function of grain size and the spall strength achieved. The thick white lines partition the space into regions that are i) predominantly transgranular, i.e. $N_{nuc}^2/N_{nuc} \gtrsim 95\%$, ii) predominantly intergranular, i.e. $N_{nuc}^1/N_{nuc} \gtrsim 95\%$, and iii) mixed-mode.

three distinct regimes for which spall strength i) follows Hall-Petch behavior, ii) scales inversely to Hall-Petch phenomena due to the greater number density of nucleation sites introduced by grain boundaries dominating and iii) insensitivity with respect to grain size. Our theory is particularly powerful as it unravels this anomalous behavior *prior* to it being conclusively demonstrated by experiments. Furthermore, it represents the first quantitative theory of metal cavitation that seamlessly connects real-world experiments to atomistic calculations, which often differ by one or two orders of magnitude. The proposed theory may prove indispensable in bridging the implications of atomistic calculations (computationally limited to ultra-short timescales, i.e. nanoseconds) of cavitation failure to more typical laboratory and engineering conditions, thereby significantly increasing their utility for design of novel materials.

[1] E. Zwaan, S. Le Gac, K. Tsuji, and C.-D. Ohl, Phys. Rev. Lett. **98**, 254501 (2007).
[2] A. Brotchie, F. Grieser, and M. Ashokkumar, Phys. Rev. Lett. **102**, 084302 (2009).
[3] H. Nanjo, A. Shima, and T. Tsujino, Nature **320**, 516 (1986).
[4] I. Chikina and C. Gay, Phys. Rev. Lett. **85**, 4546 (2000).
[5] P. Guan, S. Lu, M. J. Spector, P. K. Valavala, and M. L. Falk, Phys. Rev. Lett. **110**, 185502 (2013).

[6] P. Murali, T. Guo, Y. Zhang, R. Narasimhan, Y. Li, and H. Gao, Phys. Rev. Lett. **107**, 215501 (2011).

[7] I. Singh, R. Narasimhan, and U. Ramamurty, Phys. Rev. Lett. **117**, 044302 (2016).

[8] R. Taleyarkhan, C. West, R. Lahey Jr, R. Nigmatulin, R. Block, and Y. Xu, Phys. Rev. Lett. **96**, 034301 (2006).

[9] F. Caupin and S. Balibar, Phys. Rev. B **64**, 064507 (2001).

[10] N. McDannold, N. Vykhodtseva, and K. Hynynen, Phys. Med. Biol. **51**, 793 (2006).

[11] T. Antoun, *Spall fracture* (Springer, 2003).

[12] E. Moshe, S. Eliezer, Z. Henis, M. Werdiger, E. Dekel, Y. Horovitz, S. Maman, I. Goldberg, and D. Eliezer, Appl. Phys. Lett. **76**, 1555 (2000).

[13] M. Versluis, B. Schmitz, A. von der Heydt, and D. Lohse, Science **289**, 2114 (2000).

[14] L. Wang, J. T.-M. Cheung, F. Pu, D. Li, M. Zhang, and Y. Fan, PloS One **6**, e26490 (2011).

[15] R. M. Canup and E. Asphaug, Nature **412**, 708 (2001).

[16] R. W. Minich, J. U. Cazamias, M. Kumar, and A. J. Schwartz, Metall. Mater. Trans. A **35**, 2663 (2004).

[17] P. Peralta, S. DiGiacomo, S. Hashemian, S.-N. Luo, D. Paisley, R. Dickerson, E. Loomis, D. Byler, K. McClellan, and H. D'Armas, Int. J. Damage Mech. **18**, 393 (2009).

[18] L. Wayne, K. Krishnan, S. DiGiacomo, N. Kovvali, P. Peralta, S. Luo, S. Greenfield, D. Byler, D. Paisley, K. McClellan, *et al.*, Scr. Mater. **63**, 1065 (2010).

[19] J. Escobedo, D. Dennis-Koller, E. Cerreta, B. Patterson, C. Bronkhorst, B. Hansen, D. Tonks, and R. Lebensohn, J. Appl. Phys. **110**, 033513 (2011).

[20] T. Chen, Z. Jiang, H. Peng, H. He, L. Wang, and Y. Wang, Strain **51**, 190 (2015).

[21] F. Louchet, J. Weiss, and T. Richeton, Phys. Rev. Lett. **97**, 075504 (2006).

[22] Q. Yu, Z.-W. Shan, J. Li, X. Huang, L. Xiao, J. Sun, and E. Ma, Nature **463**, 335 (2010).

[23] D. Kiener, P. Hosemann, S. Maloy, and A. Minor, Nature Mater. **10**, 608 (2011).

[24] J. Schiøtz, F. D. Di Tolla, and K. W. Jacobsen, Nature **391**, 561 (1998).

[25] V. Yamakov, D. Wolf, S. Phillpot, A. Mukherjee, and H. Gleiter, Nature Mater. **3**, 43 (2004).

[26] S. Adibi, Z.-D. Sha, P. S. Branicio, S. P. Joshi, Z.-S. Liu, and Y.-W. Zhang, Appl. Phys. Lett. **103**, 211905 (2013).

[27] C. Carlton and P. Ferreira, Acta Mater. **55**, 3749 (2007).

[28] S. Razorenov, G. Ivanchihina, G. Kanel, B. Herrmann, and E. Zaretsky, in *AIP Conf. Proc.*, Vol. 955 (2007).

[29] A. Y. Kuksin, V. Stegailov, and A. Yanilkin, Phys. Solid State **50**, 2069 (2008).

[30] K. Mackenchery, R. R. Valisetty, R. R. Namburu, A. Stukowski, A. M. Rajendran, and A. M. Dongare, J. Appl. Phys. **119**, 044301 (2016).

[31] A. Molinari and T. Wright, J. Mech. Phys. Solids **53**, 1476 (2005).

[32] V. Dremov, A. Petrovtsev, P. Sapozhnikov, M. Smirnova, D. L. Preston, and M. A. Zocher, Phys. Rev. B **74**, 144110 (2006).

[33] N. A. Pedrazas, D. L. Worthington, D. A. Dalton, P. A. Sherek, S. P. Steuck, H. J. Quevedo, A. C. Bernstein, E. M. Taleff, and T. Ditmire, Mater. Sci. Eng. A **536**, 117 (2012).

[34] G. I. Kanel, S. V. Razorenov, and A. V. Utkin, in *High-Pressure Shock Compression of Solids II* (Springer, 1996) pp. 1–24.

[35] S. Razorenov, G. Kanel, A. Savinykh, and V. Fortov, in *AIP Conf. Proc.*, Vol. 845 (2006) pp. 650–653.

[36] H.-S. Park, R. Rudd, R. Cavallo, N. Barton, A. Arsenlis, J. Belof, K. Blobaum, B. El-dasher, J. Florando, C. Huntington, *et al.*, Phys. Rev. Lett. **114**, 065502 (2015).

[37] C. Czarnota, N. Jacques, S. Mercier, and A. Molinari, J. Mech. Phys. Solids **56**, 1624 (2008).

[38] "See supplemental material for an error analysis of Eq. (10)" .

[39] A. Bunde, S. Havlin, J. Klafter, G. Gräff, and A. Shehter, Phys. Rev. Lett. **78**, 3338 (1997).